Technical Report 1462
October 1991

Validation of the Bulk Method for Overwater Optical Refractivity

R. A. Paulus

NAVAL OCEAN SYSTEMS CENTER
San Diego, California 92152-5000

J. D. FONTANA, CAPT, USN
Commander

R. T. SHEARER, Acting
Technical Director

ADMINISTRATIVE INFORMATION

The work reported here was performed during FY 90 and 91 by the Tropospheric Branch (Code 543), Ocean and Atmospheric Sciences Division, Marine Sciences and Technology Department, for the Electromagnetic/Electro-optic Propagation block program (project SXB3), with funding provided by the Office of Naval Technology (ONT 21), 800 N. Quincy, Arlington, VA 22217.

Released by
R. A. Paulus, Head
Tropospheric Branch

Under authority of
J. H. Richter, Head
Ocean and Atmospheric
Sciences Division

ACKNOWLEDGMENTS

This work was funded by the Atmospheric Effects on EM/EO Propagation project managed by Dr. J. H. Richter in support of the Infrared Analysis, Measurement, and Modeling Program (IRAMMP). The concept for and the initiation of this experimental validation effort were the work of H. G. Hughes, now retired from the Naval Ocean Systems Center.

RH

EXECUTIVE SUMMARY

PROBLEM

Investigate effects of refraction on optical propagation at low altitudes over the ocean.

RESULTS

A telescope was used to optically track ships to the range at which they disappeared over the horizon. Concurrent bulk meteorological measurements were used with surface-layer theory to model optical refractivity. A ray-trace program, with these profiles of refractivity, was used to calculate maximum intervision range (MIVR). Calculated MIVRs agree well with observations for subrefractive conditions (air cooler than water) typical of the open ocean. Agreement is not as good for super-refractive and ducting conditions (air warmer than water), which occurred with offshore flow and are therefore not typical of open ocean. Optical ducting conditions also appear to vary with range, such that point meteorological measurements and homogeneous ray tracing are not representative.

CONTENTS

FIGURES

TABLES

1.0 INTRODUCTION

The propagation of visual and infrared (IR) waves has become important in the development and use of systems operating at these wavelengths. At low elevation angles over the ocean, the effects of refraction, attenuation, and surface roughness may be significant. Variations in the mean optical refractivity gradients at low levels can cause shortening or lengthening of the horizon. High humidity and aerosol concentrations close to the ocean surface can limit performance. A wind-ruffled sea surface emits in the IR band differently than a smooth surface, yielding a different sea background as a function of wind speed.

It is the intent of this report to investigate only the refractive effects on optical propagation and determine the validity of semiempirical flux-profile relationships in calculating mean optical refractivity profiles in the first few tens of meters above the sea surface. Davidson, et al. (1981), found reasonable agreement between optical measurements of the refractive index structure function and values determined from bulk meteorological measurements and flux-profile relationships. Low-level radiowave refractivity profiles, commonly referred to as evaporation ducts, have found widespread use in radiowave propagation. Thus there is considerable confidence that the optical refractivity profiles will be representative of real conditions.

2.0 BACKGROUND

2.1 LINEAR REFRACTIVITY MODEL

From strictly geometrical considerations, figure 1 shows

$$(h_o + a)^2 = d_g^2 + a^2 \tag{1}$$

where a is the radius of the Earth (6371 km), h_o is the altitude of the observer above the Earth, and d_g is the distance to the tangent point (geometrical horizon). If $h_o^2 << 2ah_o$, then the horizon range is

$$d_g = 3.57\sqrt{h_o} \text{ km} \tag{2}$$

where h_o is in meters.

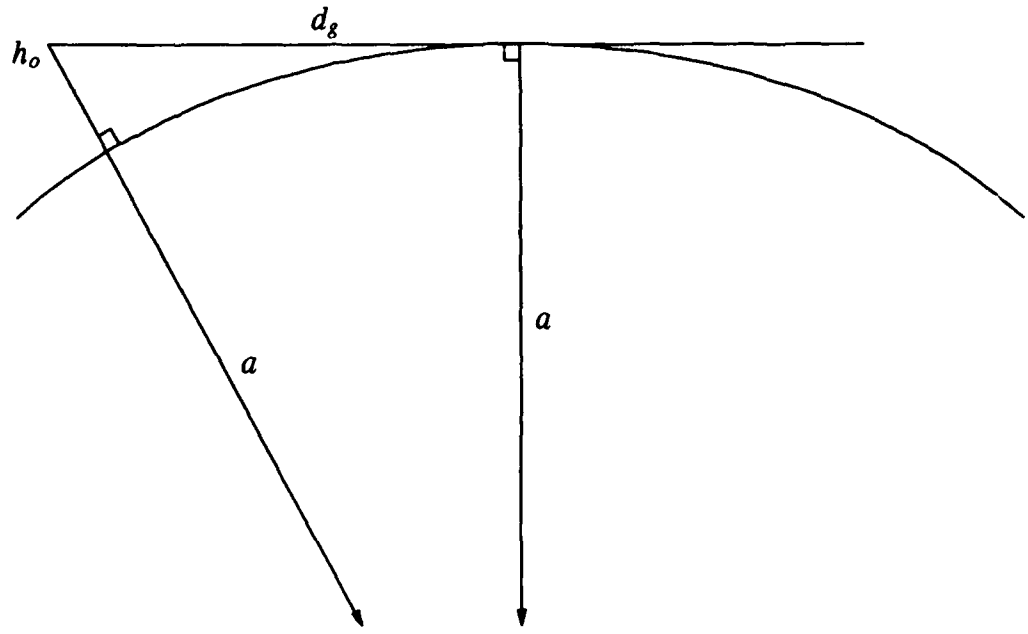

Figure 1. Geometrical horizon d_g for height of observer h_o and Earth radius a.

A more realistic version of equation 2 can be derived from ray theory for an effective Earth's radius, $a_e = ka$, where

$$k = \left(1 + a \frac{dn}{dh}\right)^{-1} \tag{3}$$

is a factor dependent on refractive index, n, that multiplies the Earth's radius to make ray trajectories straight lines (Reed and Russell, 1964; Bean and Dutton, 1968). Thus the optical horizon is now

$$d_o = 3.57\sqrt{k\, h_o} \text{ km.} \tag{4}$$

For optical wavelengths, refractivity, N, can be determined from meteorological measurements (*Handbook of Geophysics*, 1960) as

$$N = (n - 1)\, 10^6 = \left(77.6 + \frac{0.584}{\lambda^2}\right) \frac{P}{T} \tag{5}$$

where λ is wavelength (μm), P is pressure (mb), and T is temperature (K). At visible wavelengths (0.55 μm) and a standard atmosphere lapse rate of temperature, $k = 1.21$; for an adiabatic lapse rate of temperature, $k = 1.18$ (appendix A), and

$$d_o \cong 3.9\sqrt{h_o} \text{ km} \tag{6}$$

to within 1% for both lapse rates. Equation 6, in English units, has been found to be of practical use in the Navy to estimate the distance to the visible horizon (Bowditch, 1984).

Feinberg et al. (1979) investigated the refractive effects on a CO_2 laser beam propagating at low altitude over an 8.5-km path across San Diego Bay. For the prevailing conditions of water temperature warmer than air temperature, the effective Earth radius model yielded

$$d_o \cong 2.15\sqrt{h_o} \text{ km} \tag{7}$$

or about 55% of the expected optical horizon. This is indicative of subrefraction. The opposite condition, air warmer than water, would be indicative of optical superrefraction or ducting; this condition was not observed during the experiment.

2.2 LOG-LINEAR REFRACTIVITY MODEL

Feinberg's linear model of refractivity is a good approximation in the lowest part of the atmospheric boundary layer, also referred to as the surface layer. However, it can be refined by using the log-linear profile characterization of conservative scalar quantities in the surface layer (Panofsky and Dutton, 1984). For refraction, potential refractivity, N_p, is the appropriate scalar and

$$N_p = \left(77.6 + \frac{0.584}{\lambda^2}\right)\frac{P_o}{\theta} \tag{8}$$

where P_o is a reference pressure (taken here as 1000 mb) and θ is potential temperature (K) defined by

$$\theta = T\left(\frac{P_o}{P}\right)^{0.286}. \tag{9}$$

The expression for the profile of potential refractivity is

$$N_p(z) = N_p(0) + \frac{N_{p^*}}{\kappa}\left[ln\left(\frac{z + z_0}{z_0}\right) - \psi\left(\frac{z}{L}\right)\right] \tag{10}$$

which follows the equation for scalars given by Panofsky and Dutton. Here, κ is von Karman's constant (0.4), z is altitude (m), and z_0 is the aerodynamic surface roughness parameter, assumed to be constant (1.5×10^{-4} m). L is the Monin-Obukhov stability length and ψ is an empirical stability function used here as

$$\psi = -5.2\frac{z}{L} \qquad \text{for } \frac{z}{L} \geq 0$$

$$\psi = 2\,ln\left[\frac{1}{2}\left(1 + \sqrt{1 - 16\,z/L}\right)\right] \quad \text{for } \frac{z}{L} < 0\,. \tag{11}$$

N_{p^*} is the potential refractivity scaling parameter found from equation 10 as

$$N_{p^*} = \frac{\kappa\,[N_p(z_r) - N_p(0)\,]}{ln\left(\frac{z_r + z_0}{z_0}\right) - \psi\left(\frac{z_r}{L}\right)} \tag{12}$$

where z_r is a reference height at which N_p and L are determined from meteorological measurements along with N_p at the sea surface. For propagation purposes, refraction is most conveniently expressed in terms of modified refractivity, M, and the relation between M and N_p is (appendix B)

$$M(z) = N_p(z) + 0.134\,z\,. \tag{13}$$

Equation 10 then becomes

$$M(z) = M_0 + 0.134\,z + \frac{N_{p^*}}{\kappa}\left[\,ln\left(\frac{z + z_0}{z_0}\right) - \psi\left(\frac{z}{L}\right)\right]. \tag{14}$$

Using a bulk measurement approach analogous to radio refractivity (Paulus, 1989), stability and the profile of modified optical refractivity can be determined.

2.3 MAXIMUM INTERVISION RANGE

The maximum intervision range (MIVR) between a sensor and a target is the sum of the optical horizon ranges for each. In the case of linear or effective Earth radius models of refractivity, MIVR can be calculated directly.[1] In the case of the log-linear model, the easiest way to determine the optical horizon is by tracing ray trajectories. In this report, the EREPS[2] program RAYS was utilized (Patterson et al., 1990). For a given sensor altitude, RAYS traces ray paths, in height and range, based on a linearly segmented refractivity-versus-altitude profile. The optical horizon is then determined graphically as the farthest range at which a ray crosses the target altitude. Figure 2 is an example for a linear gradient of M corresponding to equation 6.

[1] Feinberg, R., H. G. Hughes, and H. V. Hitney. 1978. "Marine Boundary Layer Refractive Effects in the Infrared." NOSC TN 555. NOSC TNs (technical notes) are working documents and are not distributed outside of NOSC. For information, contact the author.

[2] Engineer's Refractive Effects Prediction System.

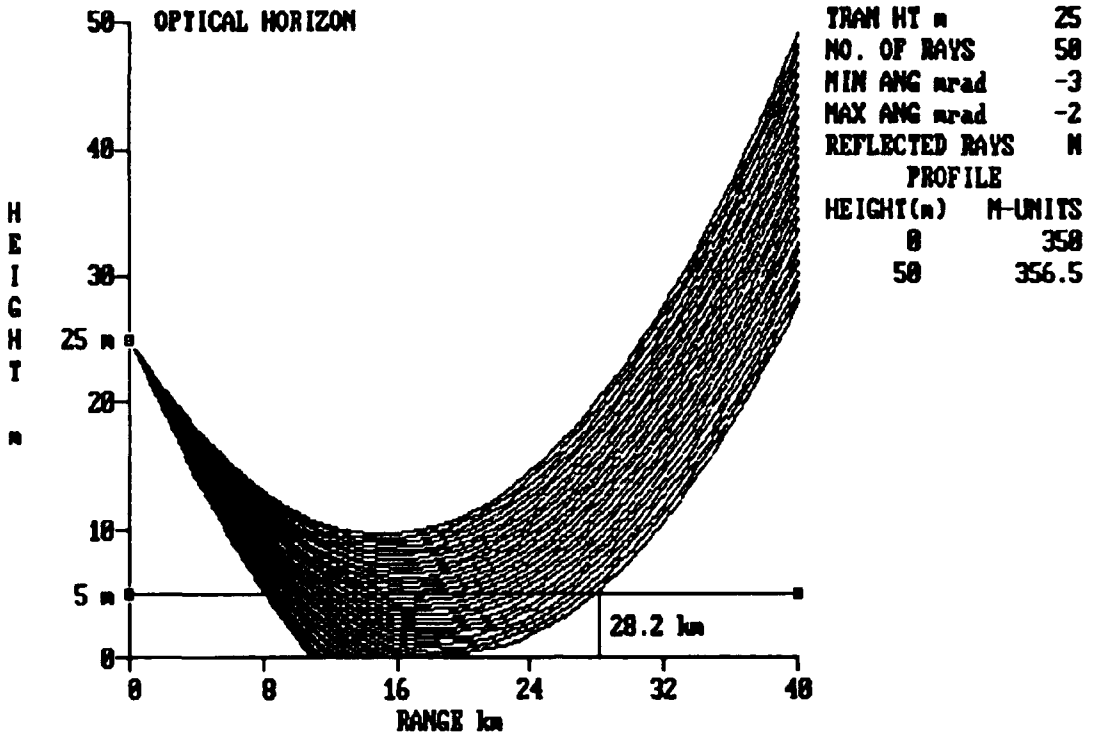

Figure 2. Optical horizon of 28.2 km determined graphically from RAYS for a 25-m sensor, a 5-m target, and a standard atmosphere (linear) gradient of M.

3.0 EXPERIMENTAL VALIDATION

The results of Feinberg and Hughes (1979) raised interest in validating the horizon changes in open-ocean conditions. Point Loma, in San Diego, is located in a prevailing northwesterly wind flow and the offshore area is generally representative of open-ocean conditions. The seaward side of the point provides access to the ocean for representative meteorological measurements, as well as the opportunity to use ships operating off the coast as possible targets of opportunity for optical tracking.

3.1 FIRST PHASE

The concept of the initial validation effort was to optically track ships leaving San Diego Bay and transiting westward over the horizon. An SPS-64 radar at the Integrated Combat Systems Test Facility on the western side of Point Loma was used to provide range to the ship versus time. Optical tracking of the ship was done with a Standard Questar 3.5-inch (89-mm) telescope set up on a tripod at an altitude of approximately 35 m above mean sea level (msl) and approximately 500 m north of the radar site at

NOSC Building 323 (figure 3). The time at which a selected target on the ship (gun mount, flight deck, or other distinctive structure) visually disappeared over the horizon was recorded and used later to determine range from the radar data logs. Meteorological data, wind speed, relative humidity, and air and sea temperature, were measured manually in the vicinity of Building 323. A computer program (appendix D) was used to calculate the M-profile for the observed meteorological data.

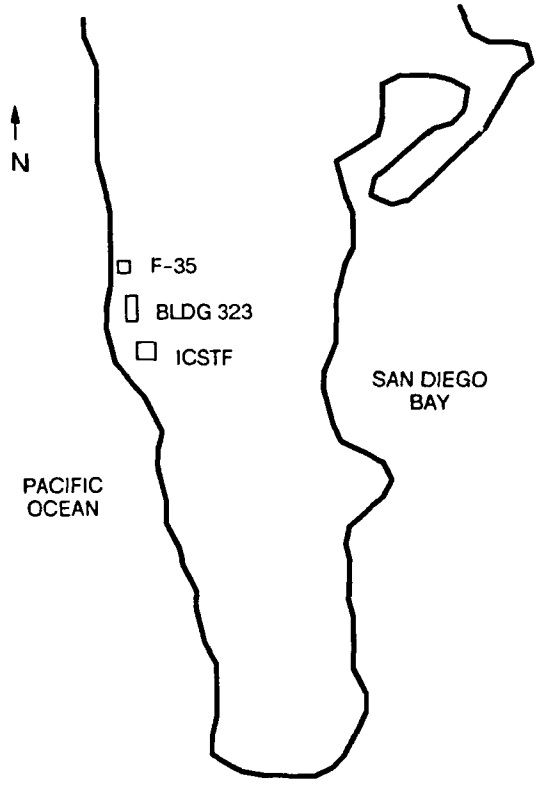

Figure 3. Point Loma experimental site.

Observations began in Spring 1990 and resulted in several problems:

1. Visibility had to be at least 30 km to visually track the ship beyond the horizon; this is not a common condition in offshore waters.

2. Contrast between the selected target on the ship and its background had to be sufficient for the observers to determine that the target had indeed disappeared beyond the horizon rather than simply fading out.

3. Using ships of opportunity introduced uncertainties into the determination of target altitude.

With these considerations, three good MIVR observations were made.

On 31 May 1990, USCGC *Munro* (WHEC 724), a *Hamilton* class cutter, was tracked. Different features of the white ship were easily tracked with the Questar. The heights of the stern (5.8 m), the helicopter landing pad (7.7 m), and the stacks (17.2 m) were determined from a USCG data sheet for the USCGC *Sherman* (WHEC 720), another *Hamilton* class cutter. These components were observed to pass over the horizon at ranges of 27.2, 28.3, and 32.8 km, respectively. From the measured meteorological data and refractivity profile (figure 4), the calculated MIVRs were 32.0, 33.7, and 39.2 km, respectively (figure 5), about 18 to 20% greater than the measurements.

On 27 August 1990, the USS *Ranger* (CV 61), which had a white stern ramp against a gray hull (21.5 m msl) as determined from *Jane's Fighting Ships* (1990), was observed to dip over the horizon at 35.6 km. Prior to passing the horizon, the white stern ramp was observed to have multiple images in the vertical, indicative of subrefraction. However, the subsequent meteorological measurements yielded a refractivity profile with a low duct (figure 6) and the calculated MIVR was 42.2 km (figure 7). Again, the range is about 19% greater than the measured MIVR, and there are no indications of mirage effects in the raytrace diagram. Measurements of sea temperature at Mission Beach (21.7°C) and Scripps Pier (22.8°C), both north of Point Loma, indicated warmer water. Using a sea temperature of 22°C yielded a subrefractive profile (figure 8), a calculated MIVR of 37.3 km (within 5% of observed), and crossing rays that would produce multiple images (figure 9). Greenler (1980) gives a qualitative description of the phenomena of mirages and multiple images, and their relation to refractive conditions.

On 7 November 1990, the USS *Leahy* (CG 16) was tracked. The selected features on the ship were the stern (5 m), the bow (10 m), and the PHALANX close-in weapon system radome (14 m). The heights of these features were determined from scale drawings in *Jane's Fighting Ships* (1990). Observed MIVRs of 26.2, 30.7, and 34.0 km were less than the calculated ranges (figures 10 and 11). The low optical duct in figure 10 was caused by a *foehn* condition over southern California (figure 12). Gossard (1982) discusses this type of condition and shows the theoretical variation of the duct with range. It is highly likely that the range variation of the duct contributed significantly to the discrepancy between observed and calculated ranges. Such inhomogeneities are not uncommon in coastal areas but are rare in the open ocean. Also apparent from figure 11 are the nearly horizontal ray trajectories over a considerable range interval (~10 km) near the angle of the critical ray that is just tangential to the top of the duct. This indicates that the calculated MIVR would be quite sensitive to small inaccuracies in the observer and target altitudes.

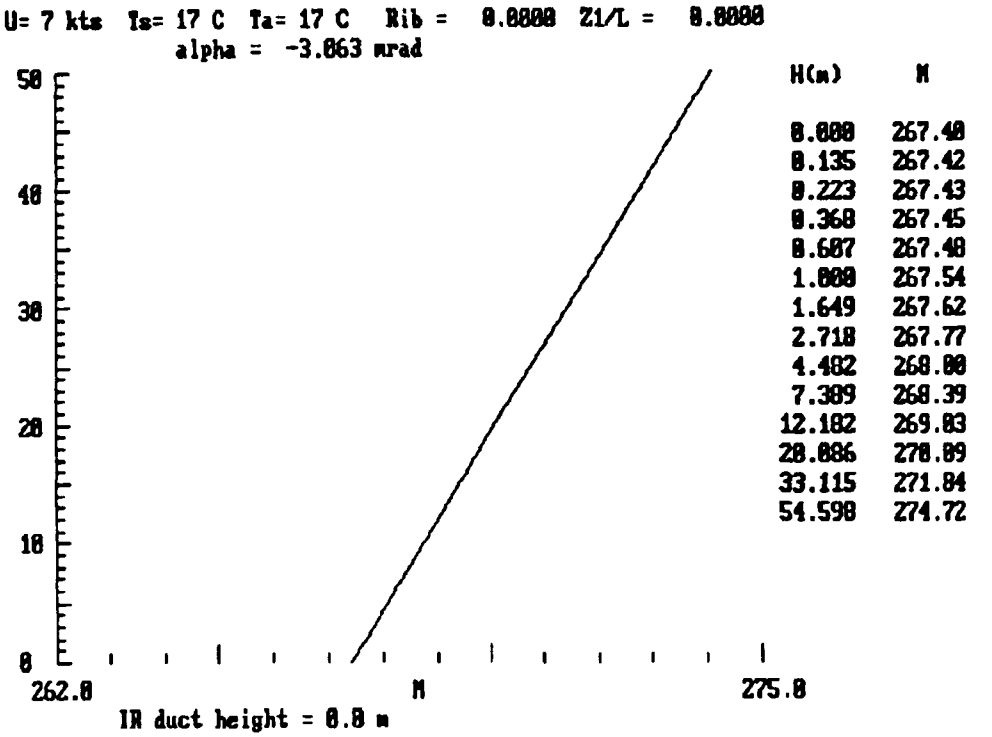

Figure 4. Bulk meteorological data and calculated optical refractivity at the time of the MIVR observation of USCGC *Munro* (WHEC 724).

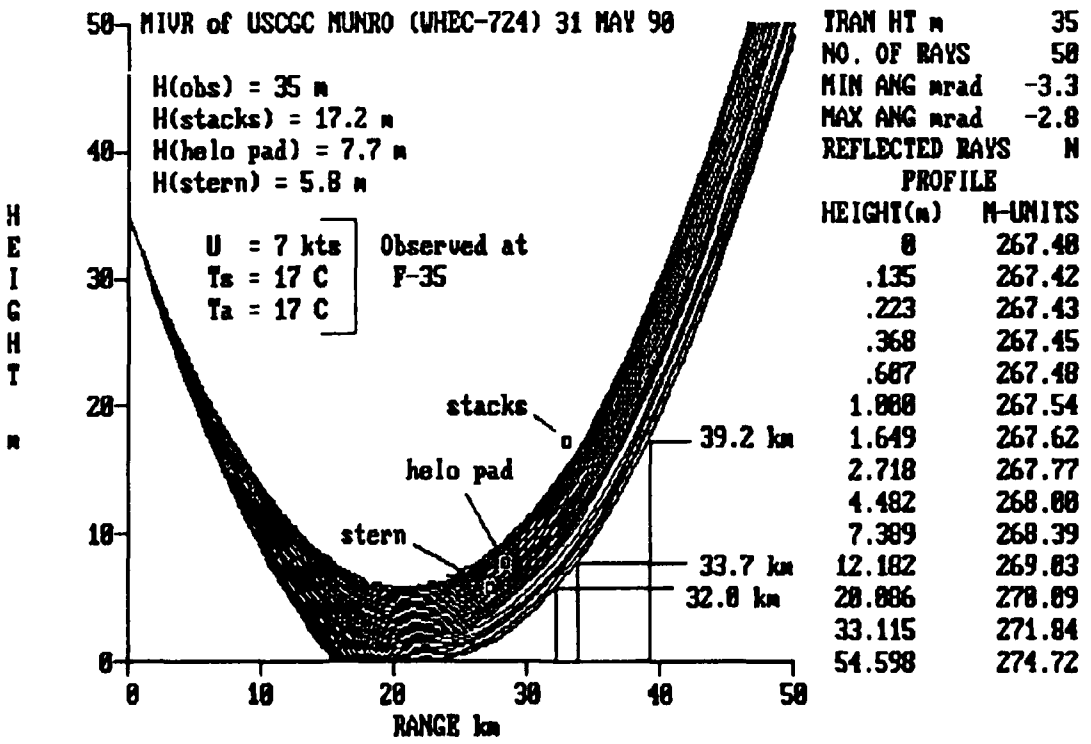

Figure 5. EREPS RAYS display for refractivity profile of figure 4.

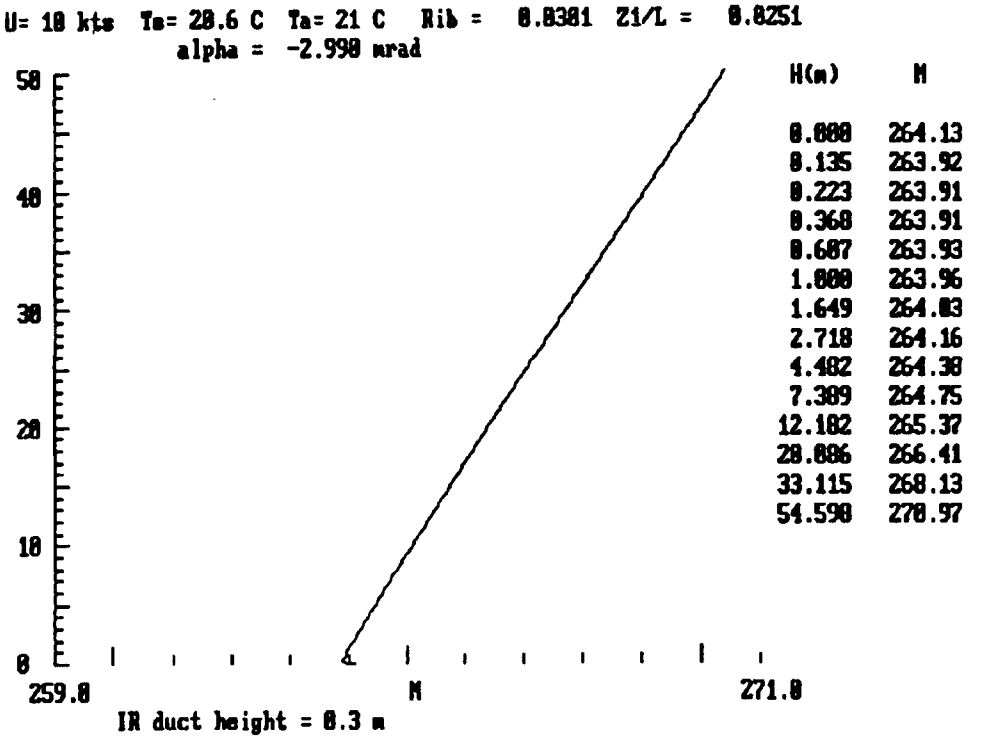

Figure 6. Bulk meteorological data and calculated optical refractivity at the time of the MIVR observation of USS *Ranger* (CV 61).

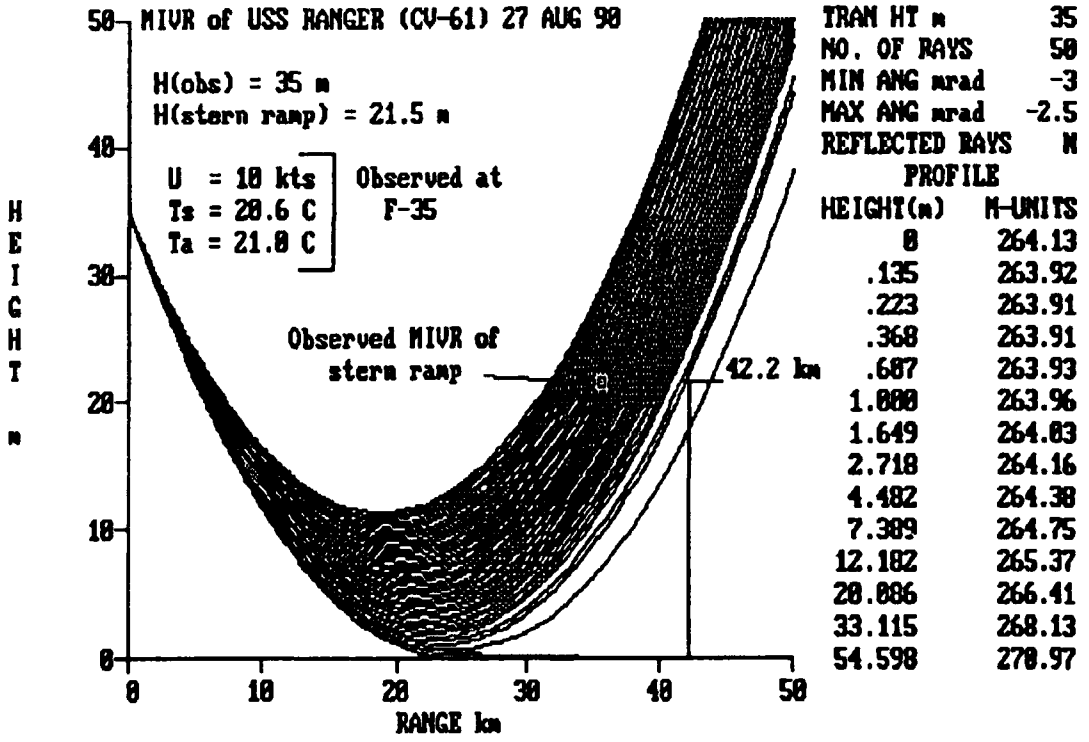

Figure 7. EREPS RAYS display for refractivity profile of figure 6.

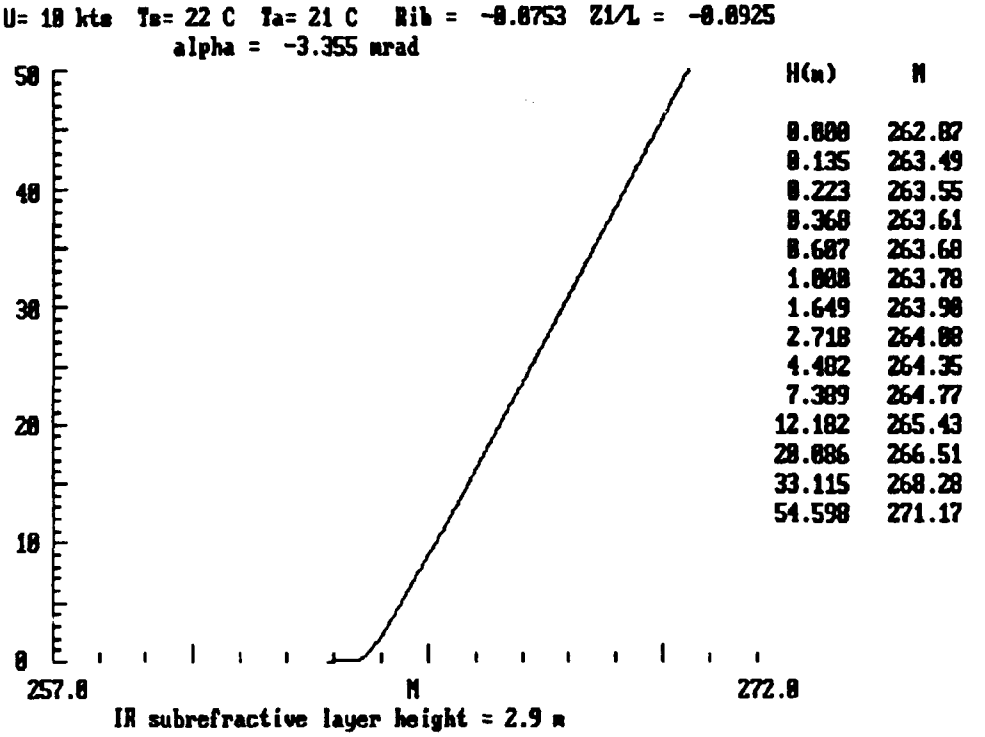

Figure 8. Optical refractivity profile based on the bulk meteorological data of figure 6 except using a sea temperature of 22°C.

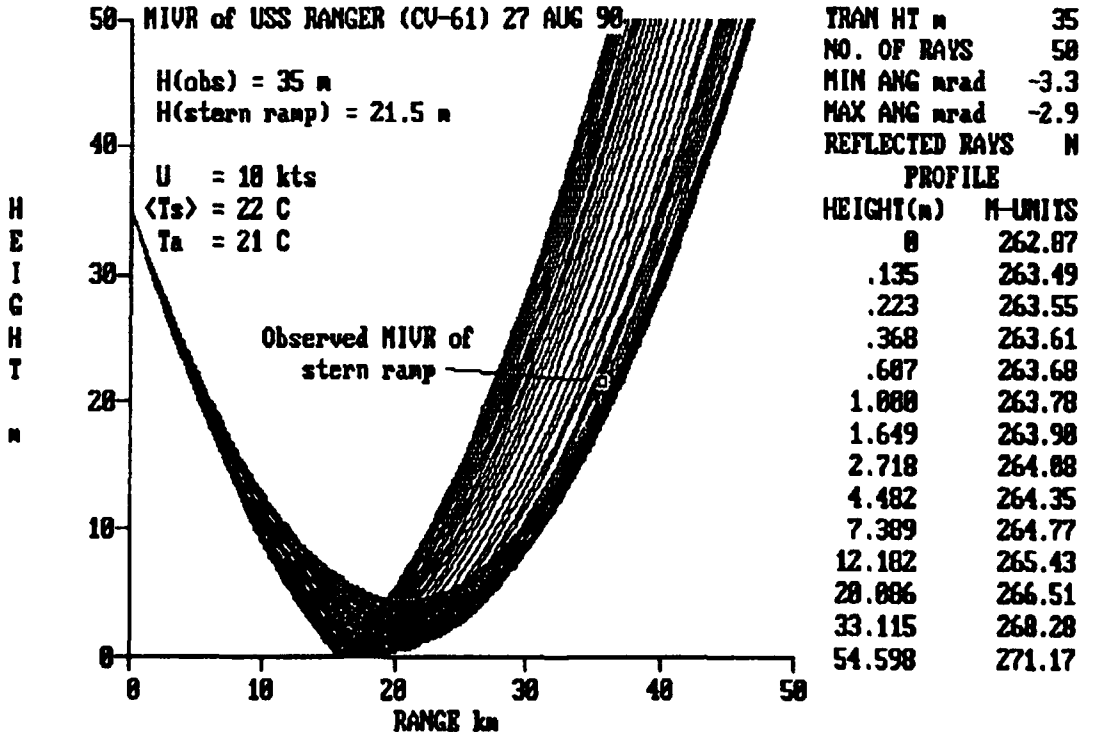

Figure 9. EREPS RAYS display for refractivity profile of figure 8.

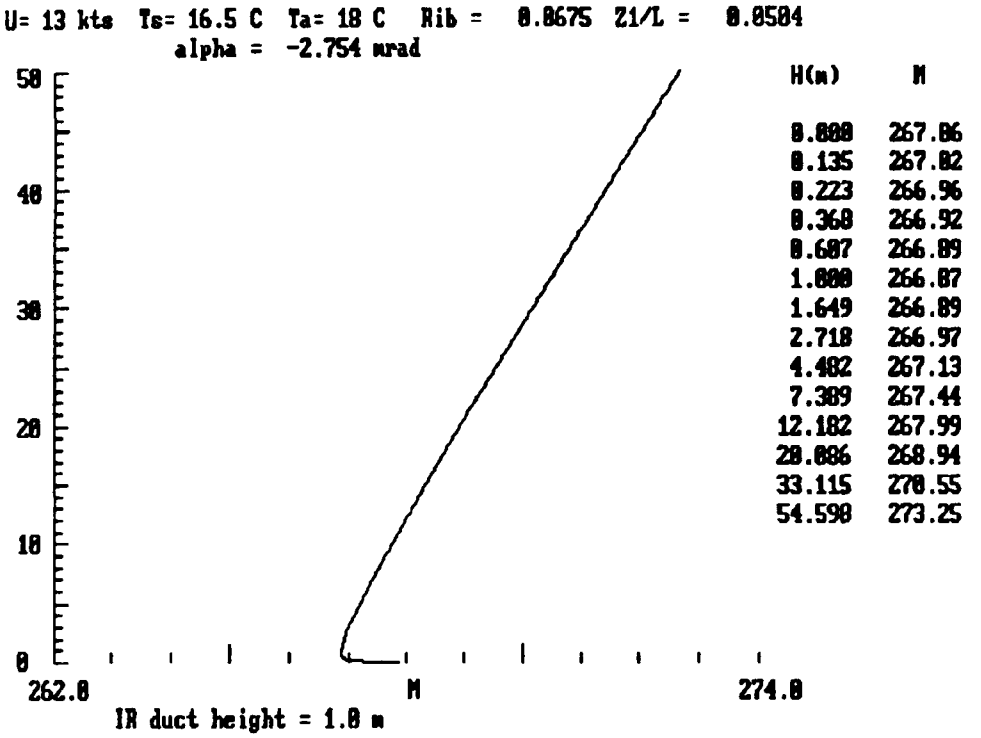

Figure 10. Bulk meteorological data and calculated optical refractivity at the time of the MIVR observation of USS *Leahy* (CG 16).

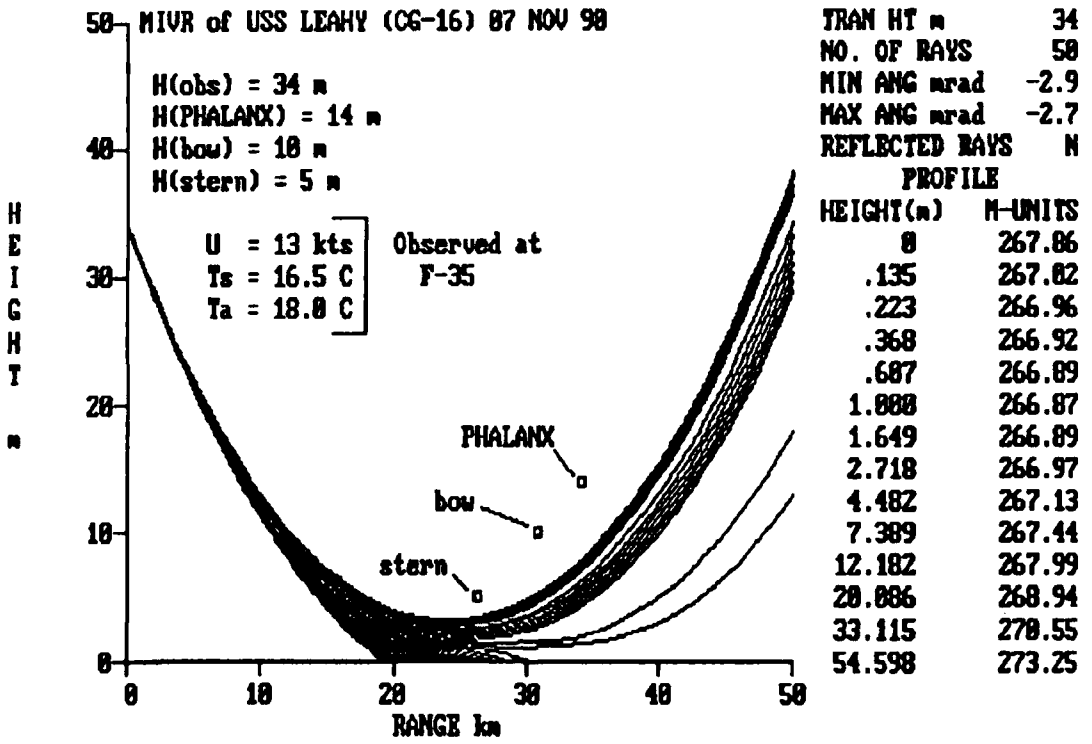

Figure 11. EREPS RAYS display for refractivity profile of figure 10.

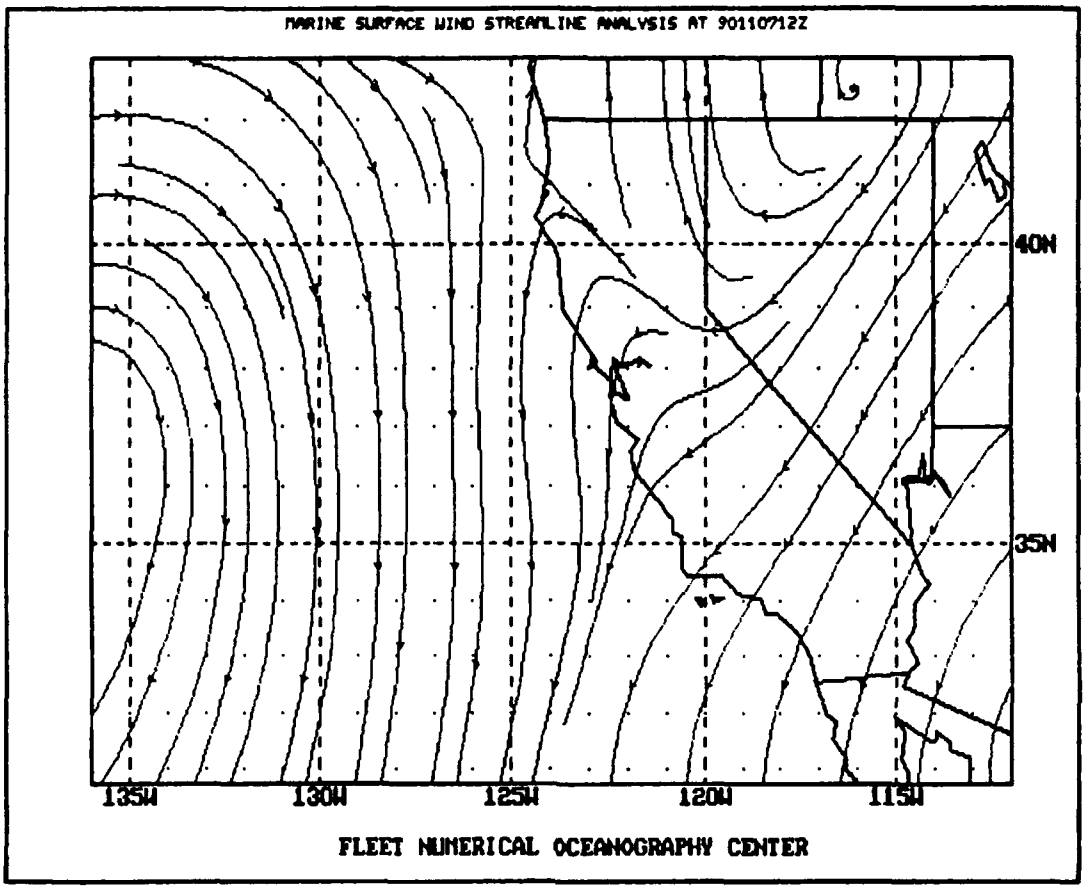

Figure 12. Synoptic-scale offshore wind flow shown by 1200Z 7 November 1990 streamline analysis obtained from Fleet Numerical Oceanography Center via the Naval Oceanographic Data Distribution System (NODDS).

3.2 SECOND PHASE

The lack of success in the initial attempt to collect MIVRs and validate the bulk-derived refractivity profiles led to a more controlled experimental approach. An experimental measurement program to determine the effects of the evaporation duct on low-altitude propagation began in October 1990 (Anderson, 1991). This experiment involved radar tracking of a small, high-speed boat carrying forward- and aft-facing triangular corner reflectors on radials away from and towards a radar located at site F-35 on Point Loma (figure 3). Meteorological data were measured in an instrument shelter on a platform overlooking the ocean near the radar and on the target boat by redundant sensors and manual observations. Intercomparisons of the meteorological sensors prior to each data collection period provided accurate relative measurements, a primary concern in making bulk measurements to determine surface-layer profiles. In addition, radiosondes were released to provide data at higher levels.

Joining in on this experiment involved only setting up the telescope near the radar site. The corner reflectors and the hull of the chartered boat (named *Miami Vice*) were used as the optical targets. The hull extended 1.2 m above the water and the corner reflectors were mounted 5 m above the water. The limitations of visibility and target/background contrast mentioned above remained. This brought up the question of whether the telescope could resolve the corner reflectors at horizon ranges on the order of 20 to 30 km. Calculations in appendix C show that the telescope could easily resolve these targets, visibility permitting. However, optical turbulence could be expected to cause a shimmering of the target image.

Figures 13 to 19 show the MIVR calculations for 7 days of successful observations. MIVRs are summarized in table 1. The telescope was mounted at the F-35 site near the radar at an altitude of 21.9 m msl. The observer height was corrected for the tide level at the time of the observation. Meteorological data used to generate the optical refractivity profiles were those manually observed data at the F-35 site closest in time to the MIVR observation. Although the optical target altitudes were now well known, the small boat was far more susceptible to wave motion than the larger ships tracked earlier. The effect on determining MIVR was an extended range at the horizon over which the target would appear and disappear as the boat crested the waves and dropped into the troughs. This is indicated in figures 17 to 19 by the two markers joined by a line at each target altitude. In addition, multiple images were commonly observed. Of the 7 days, 2 days had an optical duct and the wind direction was northerly, indicating a recent overland trajectory. The remaining days had subrefractive conditions with westerly to northwesterly winds indicative of long overwater trajectories. On 18 December and 16 January, an aircraft strobe light was mounted below the corner reflector in an unsuccessful attempt to overcome the visibility and contrast problems and still have a small optical target. Thus, only on the 3 days in March did the visibility permit tracking the corner reflector until it definitely disappeared over the horizon. Conversely, only on these 3 days was the boat able to be tracked optically on the inbound leg since the higher corner reflector provided a cue as to where the boat was before the hull appeared.

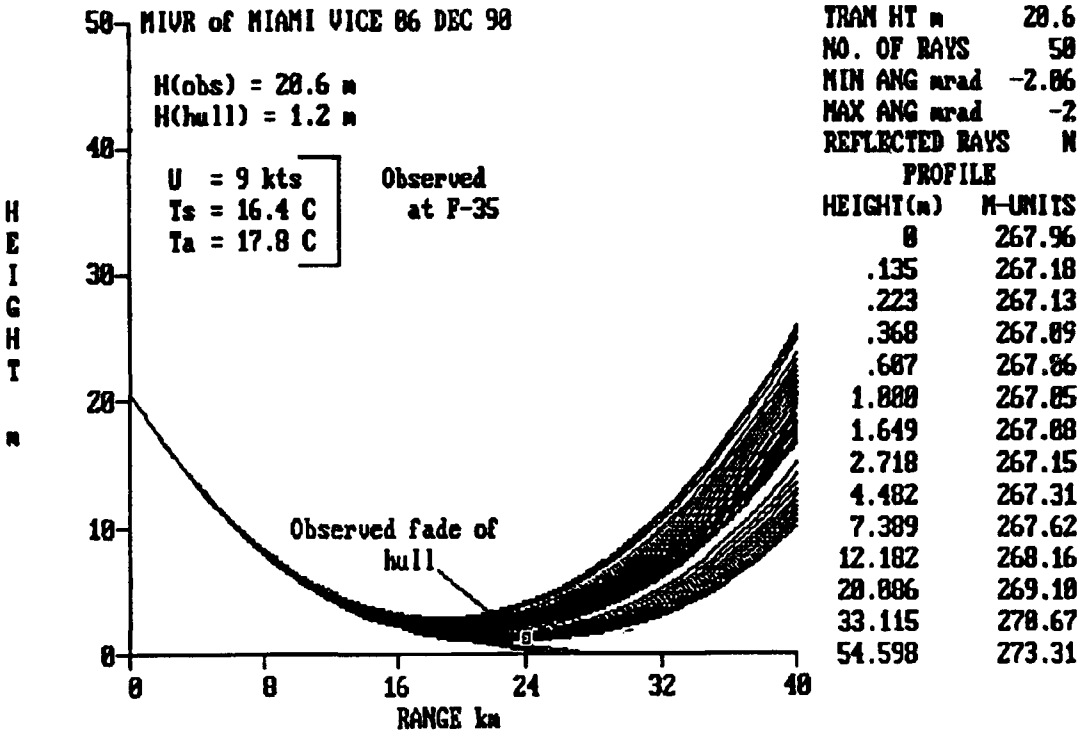

Figure 13. EREPS RAYS ray-trace analysis of MIVR for *Miami Vice* on 6 December 1990.

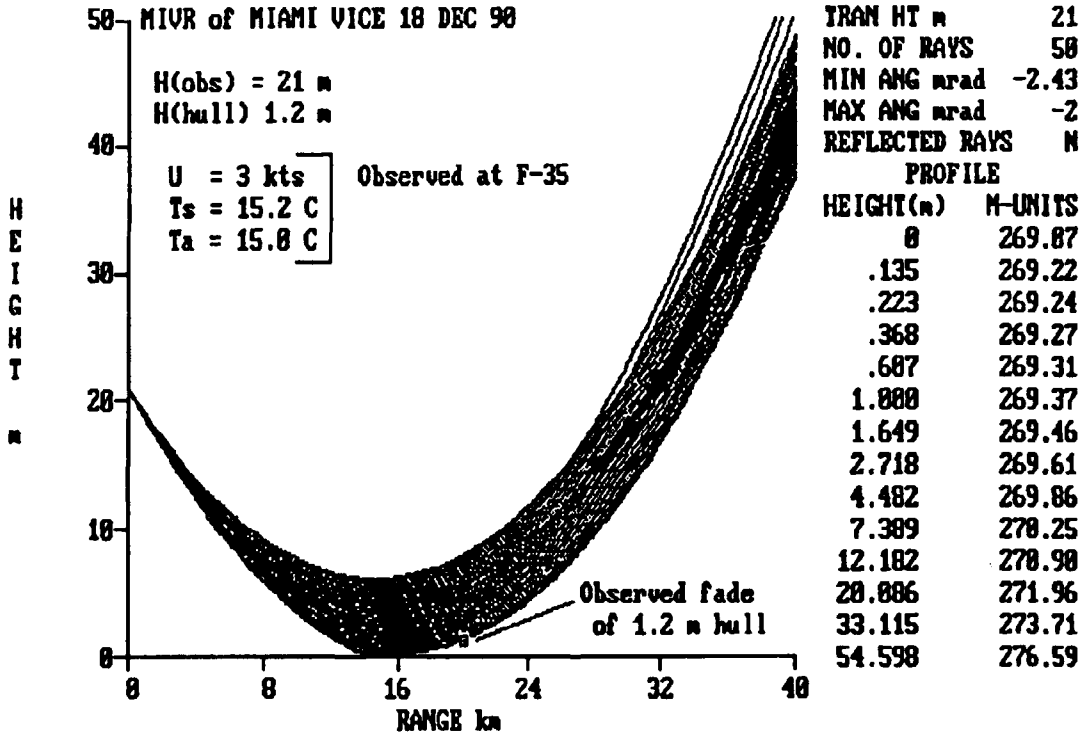

Figure 14. EREPS RAYS ray-trace analysis of MIVR for *Miami Vice* on 18 December 1990.

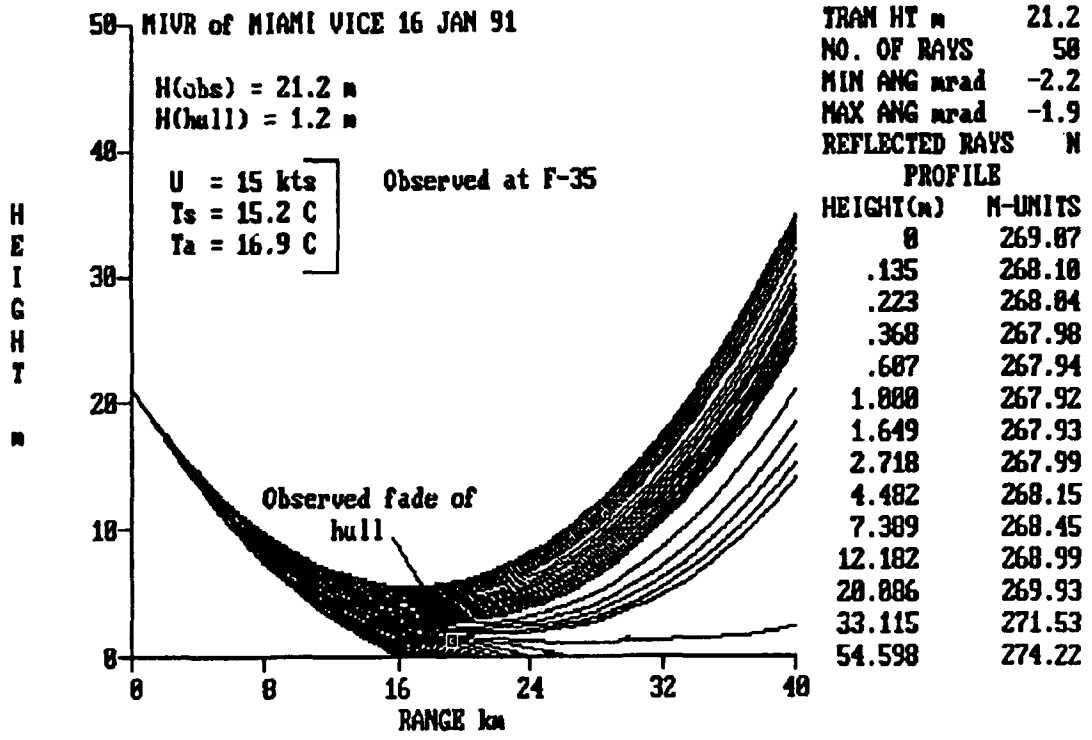

Figure 15. EREPS RAYS ray-trace analysis of MIVR for *Miami Vice* on 16 January 1991.

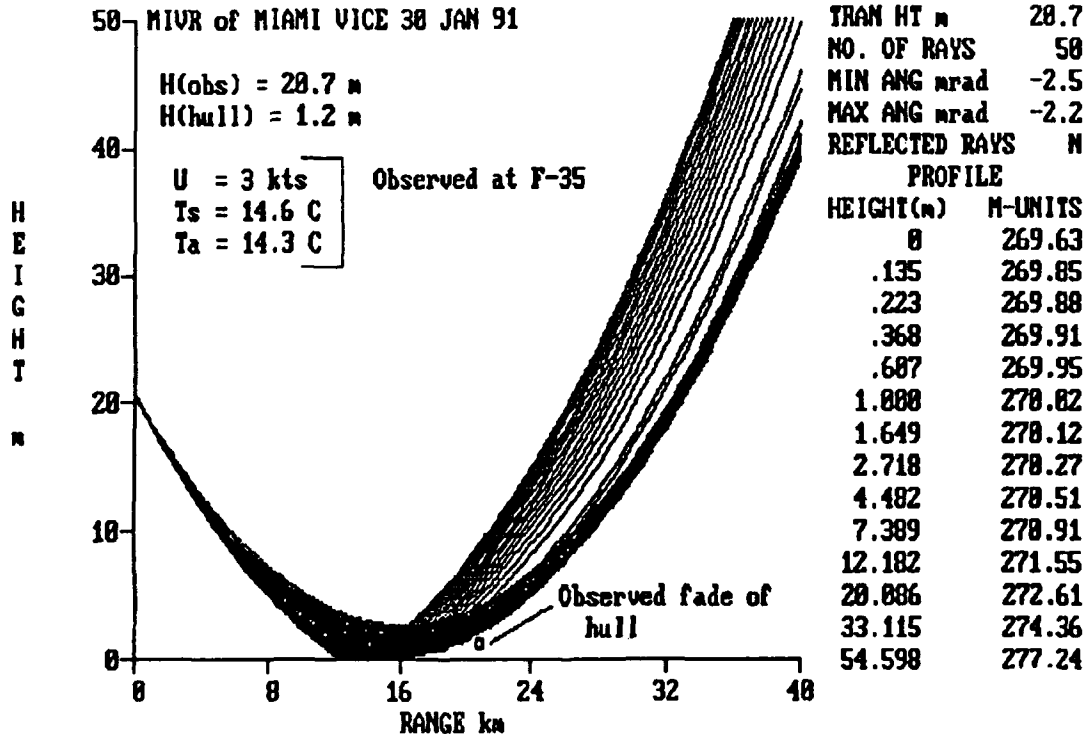

Figure 16. EREPS RAYS ray-trace analysis of MIVR for *Miami Vice* on 30 January 1991.

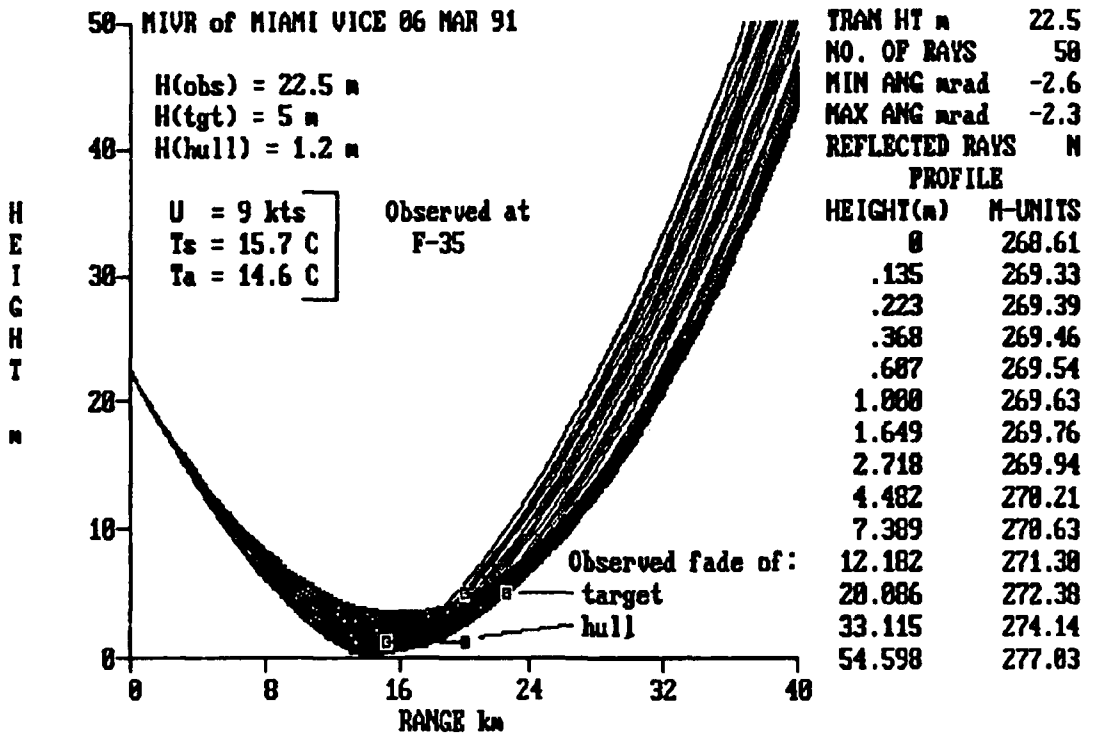

Figure 17. EREPS RAYS ray-trace analysis of MIVR for *Miami Vice* on 6 March 1991.

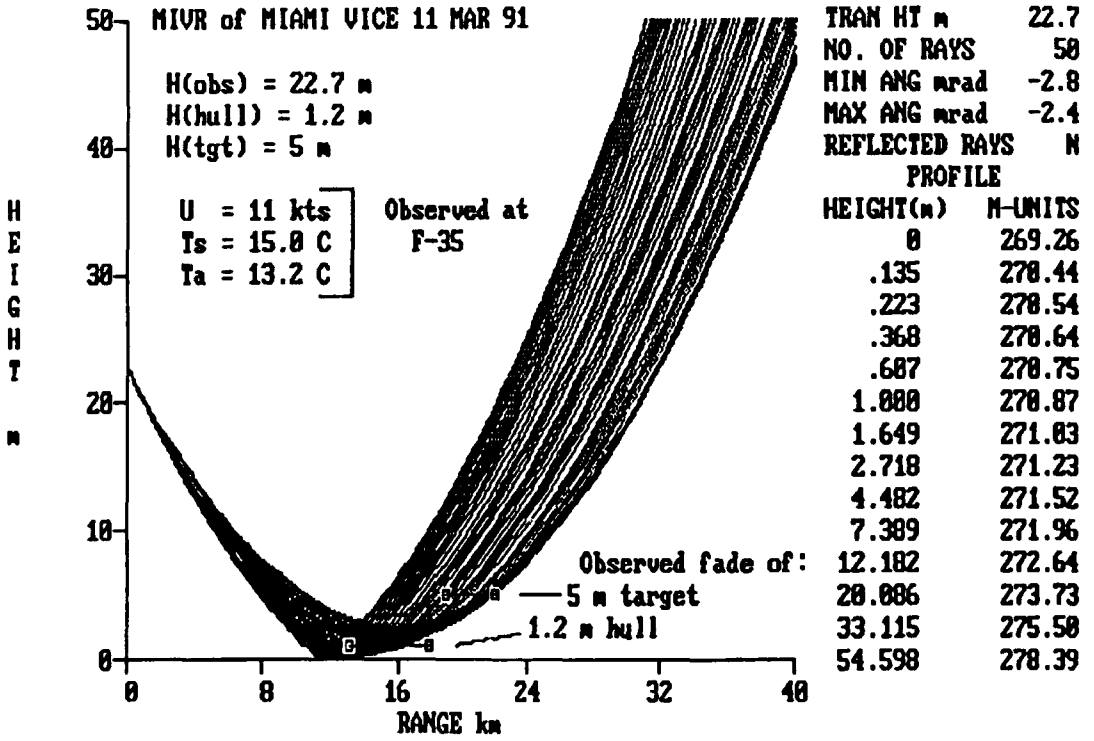

Figure 18. EREPS RAYS ray-trace analysis of MIVR for *Miami Vice* on 11 March 1991.

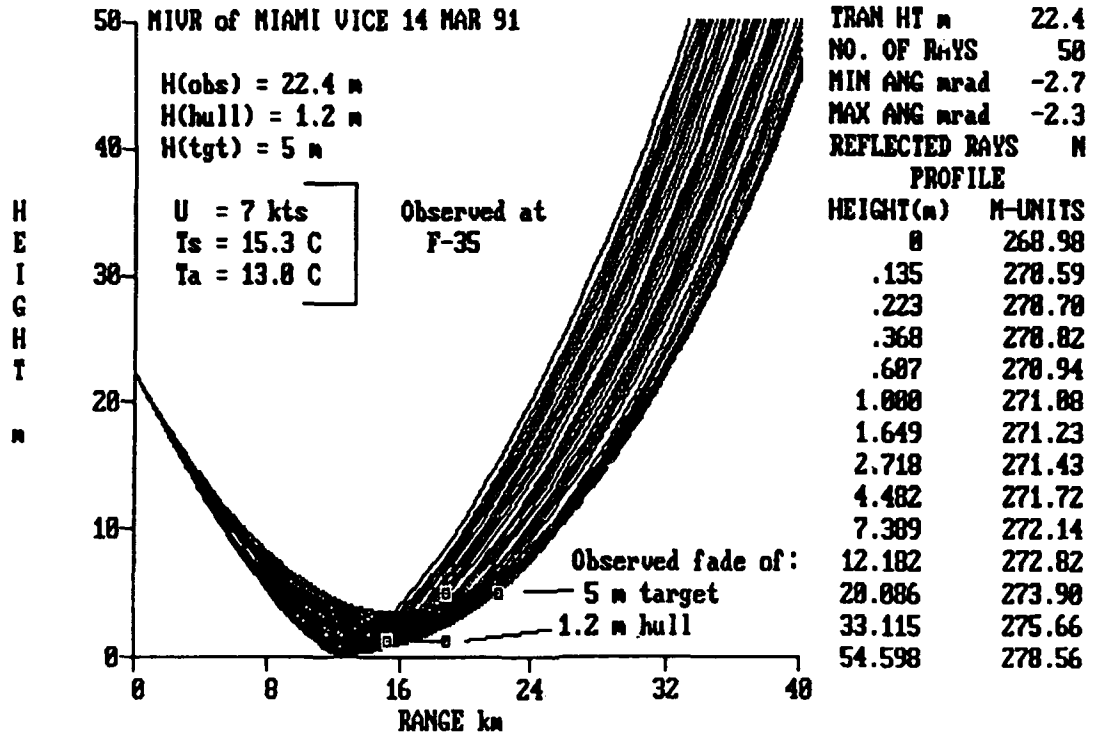

Figure 19. EREPS RAYS ray-trace analysis of MIVR for *Miami Vice* on 14 March 1991.

Table 1. Calculated and observed MIVRs for the *Miami Vice*. Out and in refer to observation during the outbound and inbound legs, respectively.

Date	H(obs) (m)	MIVR of Hull (km)		MIVR of Corner Reflector (km)	
		Observed	Calculated	Observed	Calculated
06 Dec 90	20.6	23.9 (out)	26.4	–	–
18 Dec 90	21.0	20.1 (out)	20.1	–	–
16 Jan 91	21.2	19.2 (out)	23.2	–	–
30 Jan 91	20.7	20.9 (out)	19.9	–	–
06 Mar 91	22.5	20.2 (out)	18.4	22.6	22.9
		19.4 (in)	18.4	–	–
11 Mar 91	22.7	17.9 (out)	17.0	22.0	22.0
		17.0 (in)	17.0	–	–
14 Mar 91	22.4	18.9 (out)	17.0	22.1	22.0
		18.0 (in)	17.0	–	–

3.3 RESULTS

Calculated and observed MIVRs of the corner reflectors are in good agreement (< 5% difference between observed and calculated). On the 5 subrefractive days, calculated and observed MIVRs on the hull were within 10%. Observed MIVRs for the hull were consistently farther than calculated, and inbound MIVRs were consistently less than outbound. This may be the result of spray being tossed up as the boat crests a wave and being mistakenly observed as the hull. Outbound runs were always into the seas and inbound runs always had following seas. On the two days of optical ducting, observed MIVRs were consistently greater than calculated, probably because of range-dependent variations in the optical refractivity profiles, as discussed earlier. Only on 6 December 90 were meteorological data for a ducting condition available, in range, from the boat. Figure 20 shows a portion of these data. The time period of interest for the MIVR observation is 1136 to 1205 PST. During this interval, the air-sea temperature difference varied between +1.7°C maximum and +0.4°C minimum in a range interval from 3.6 to 27.5 km from the F-35 radar site. Spikes in the air temperature trace were disregarded. Averaging meteorological data over a few kilometers on either side of the points of change indicated by arrows in figure 20 yields the variations in optical duct height shown in table 2. Although beyond the scope of the current study, the range variation of optical refractivity could be taken into account with techniques like Patterson's (1987).

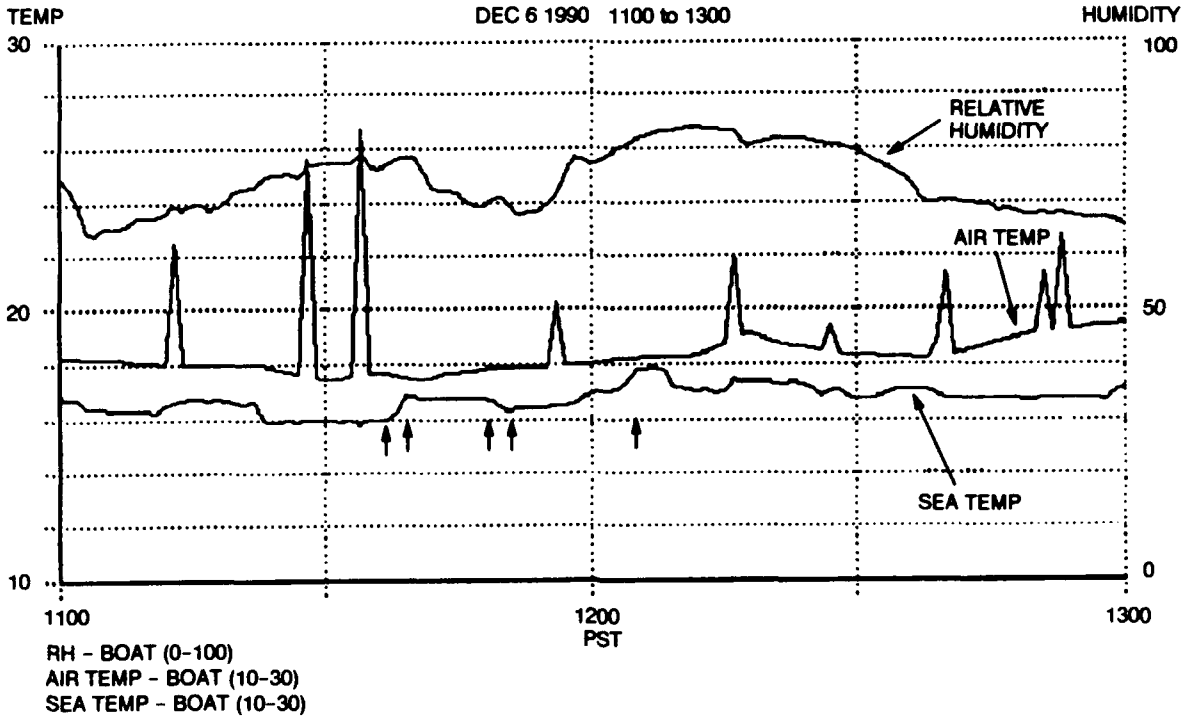

Figure 20. Sea temperature, air temperature, and relative humidity recorded on *Miami Vice* 6 December 1990.

Table 2. Optical duct height versus range.

Optical Duct Height (m)	Range (km)
0.8	0
1.1	4
0.4	6
0.7	13
1.1	16
0.7	25

4.0 CONCLUSIONS

Atmospheric attenuation (aerosol scattering and absorption) is a significant effect in limiting optical ranges to less than the MIVR under open-ocean conditions. Many ships of opportunity and *Miami Vice* runs were missed because of degraded optical conditions.

Carefully measured bulk meteorological data and surface-layer flux-profile relationships provide a representative refractivity profile for MIVR calculations for open-ocean conditions. These conditions are predominantly air temperature cooler than that of water, and are thus subrefractive for optical and IR wavelengths.

Optical ducting, expected to be rare in the open ocean, can occur routinely in coastal regions with offshore flow. Ray tracing in this situation is sensitive to the observer/target geometry, and it is very likely that the refractive conditions are variable in range. Thus simple point measurements and homogeneous ray tracing will not be applicable. Optical ducting could conceivably produce extended optical ranges for very low-sited sensors and targets, atmospheric attenuation permitting. The geometry of this experiment did not permit resolving this question, although examples of this phenomenon have been published by Greenler (1980) and others.

REFERENCES

Anderson, K. D. 1991. "Remote sensing of the evaporation duct using an X-band radar," *Proceedings of the 49th AGARD-EPP Symposium on Remote Sensing of the Propagation Environment*. 30 Sep - 4 Oct 1991. Cesme, Turkey. In preparation.

Bean, B. R., and E. J. Dutton. 1968. *Radio Meteorology*. Dover Publications, Inc., New York.

Bowditch, N. 1984. *American Practical Navigator*, vol. 1, appendix T. Defense Mapping Agency Hydrographic/Topographic Center, Washington, DC.

Davidson, K. L., G. E. Schacher, C. W. Fairall, and A. K. Goroch. 1981. "Verification of the bulk method for calculating overwater optical turbulence," *Applied Optics*, vol. 20, no. 17, pp. 2919 - 2924.

Feinberg, R., and H. G. Hughes. 1979. "Marine boundary layer refractive effects in the infrared," *Applied Optics*, vol. 18, no. 15, pp. 2532-2534.

Fleagle, R. G., and J. A. Businger. 1980. *An Introduction to Atmospheric Physics*, p. 351. Academic Press, New York.

Gossard, E. E. 1980. "Formation of elevated refractive layers in the oceanic boundary layer by modification of land air flowing offshore," *Radio Science*, vol. 17, no. 2, pp. 385-398.

Greenler, R. 1980. *Rainbows, Halos, and Glories*. Chapter 7. Cambridge University Press, Cambridge, U. K.

Halliday, D., and R. Resnick. 1962. *Physics*, pp. 1112-1115. John Wiley and Sons, New York.

Handbook of Geophysics. 1960. U. S. Air Force Cambridge Research Center, MacMillan, New York. Chapter 13.

Jane's Fighting Ships. 1990. CAPT Richard Sharpe, RN, editor. Jane's Publishing Company Limited, New York.

Panofsky, H. A., and J. A. Dutton. 1984. *Atmospheric Turbulence*. John Wiley and Sons, New York.

Patterson, W. L. 1987. "A Raytrace Method for a Laterally Heterogeneous Environment," NOSC TR 1180 (July). Naval Ocean Systems Center, San Diego, CA.

Patterson, W. L., C. P. Hattan, H. V. Hitney, R. A. Paulus, A. E. Barrios, G. E. Lindem, and K. D. Anderson. 1990. "Engineer's Refractive Effects Prediction System (EREPS) Revision 2.0," NOSC TD 1342 (February). Naval Ocean Systems Center, San Diego, CA.

Paulus, R. A. 1989. "Specification for Environmental Measurements to Assess Radar Sensors," NOSC TD 1685, (November). Naval Ocean Systems Center, San Diego, CA.

Reed, H. R., and C. M. Russell. 1964. *Ultra High Frequency Propagation*. Boston Technical Publishers, Boston, MA.

APPENDIX A

REPRESENTATIVE LINEAR GRADIENTS OF REFRACTIVITY

The vertical derivative of optical refractive index at 0.55 μm is

$$\frac{dN}{dz} = 79.5\left(\frac{T\,dP/dz - P\,dT/dz}{T^2}\right) m^{-1} . \qquad \text{(A-1)}$$

The vertical derivative of pressure can be approximated by assuming hydrostatic equilibrium, $dP/dz = -\rho g$, and then, by the equation of state,

$$\frac{dP}{dz} = -\frac{P\,g}{R\,T}\ mb/m \qquad \text{(A-2)}$$

where ρ is density, g is acceleration of gravity (9.8 m/s2), P is pressure (taken to be 1000 mb), R is the individual gas constant for dry air (2.87×10^6 erg/g/K), and T is temperature (K). This yields a variation of dP/dz from −0.12 to −0.11 mb/m over the temperature range of 0 to 30°C. Taking standard temperature (15°C) and standard atmosphere temperature lapse rate (−6.5°C/km),

$$\frac{dN}{dz} = -0.027\ m^{-1} . \qquad \text{(A-3)}$$

Over the ocean, the atmosphere is often well mixed in the boundary layer and an adiabatic lapse of temperature exists (−10°C/km), resulting in

$$\frac{dN}{dz} = -0.024\ m^{-1} . \qquad \text{(A-4)}$$

With $dn/dz = dN/dz \times 10^{-6}$, equations A-3 and A-4 yield effective Earth radius factors of 1.21 and 1.18, respectively. For infrared wavelengths, values of the effective Earth radius factor vary less than 1%.

APPENDIX B

RELATION BETWEEN MODIFIED AND POTENTIAL REFRACTIVITY

Optical refractivity is

$$N = \left(77.6 + \frac{0.584}{\lambda^2}\right)\frac{P}{T} . \tag{B-1}$$

The total derivative with respect to z is

$$\frac{dN}{dz} = \frac{\partial N}{\partial P}\frac{dP}{dz} + \frac{\partial N}{\partial T}\frac{dT}{dz} \tag{B-2}$$

where the partial derivatives are

$$\frac{\partial N}{\partial P} = \frac{77.6 + 0.584/\lambda^2}{T}$$

$$\frac{\partial N}{\partial T} = -\frac{(77.6 + 0.584/\lambda^2)\,P}{T^2} . \tag{B-3}$$

Similarly, potential optical refractivity is

$$N_p = \left(77.6 + \frac{0.584}{\lambda^2}\right)\frac{P_o}{\theta} \tag{B-4}$$

where P_o = 1000 mb and $\theta = T\ (P_o/P)^{0.286}$. The total derivative with respect to z is

$$\frac{dN_p}{dz} = \frac{\partial N_p}{\partial \theta}\frac{d\theta}{dz} \tag{B-5}$$

where

$$\frac{\partial N_p}{\partial \theta} = -\frac{\left(77.6 + \frac{0.584}{\lambda^2}\right)P_o}{\theta^2} . \tag{B-6}$$

At 1000 mb, $N = N_p$, $T = \theta$, $\partial N/\partial T = \partial N_p/\partial \theta$, and $d\theta/dz = dT/dz + 0.01$. Substituting back into equation B-2,

$$\frac{dN}{dz} = \frac{\partial N}{\partial P}\frac{dP}{dz} - 0.01\frac{\partial N_p}{\partial \theta} + \frac{\partial N_p}{\partial \theta}\frac{d\theta}{dz} . \tag{B-7}$$

The last term on the right-hand side is dN_p/dz and with P=1000 mb, T=15 C, and λ=0.55 μm, the first two terms on the right-hand side can be evaluated to give

$$\frac{dN}{dz} = \frac{dN_p}{dz} - 0.023 \qquad \text{(B–8)}$$

or $N = N_p - 0.023\ z$. Since $M = N + 0.157\ z$,

$$M = N_p + 0.134\ z\ . \qquad \text{(B–9)}$$

This relation is valid in the surface layer, where variation in pressure away from 1000 mb is small.

APPENDIX C

QUESTAR TARGET RESOLVING CAPABILITY

Assuming Fraunhofer conditions and applying the (arbitrary) Rayleigh criterion, the resolving power of a lens (Halliday and Resnick, 1962) is approximately

$$\theta_R = 1.22 \frac{\lambda}{d} \text{ rad} . \qquad \text{(C–1)}$$

where θ_R is resolution, λ is wavelength, and d is aperture. λ and d must be in consistent units. For the Standard Questar with a 3.5-inch (88.9-mm) aperture, the resolving power should be $\theta_R = 7.5 \times 10^6$ rad = 1.6 seconds of arc. The triangular corner reflectors used in the low-altitude propagation experiment are 40 inches on a side. Conservatively approximating the triangular shape with a sphere the same diameter as the inscribed circle yields a diameter of 0.6 m. Fleagle and Businger (1980) state that an object must subtend at least 1 minute of arc for the human eye to easily resolve it. Using

$$r = s/\theta \qquad \text{(C–2)}$$

where s is arc length and θ is in radians, the range at which a 0.6-m-diameter sphere is 1 minute of arc is 2 km. Several observers verified that the corner reflector was visible at this range so that approximating it in this manner is valid. The range at which the 0.6-m sphere subtends an angle equal to the resolving power of the telescope is 77 km. Therefore, visibility permitting, the telescope should be easily capable of observing the corner reflector as it crosses the horizon.

APPENDIX D

QUICKBASIC COMPUTER PROGRAM FOR OPTICAL REFRACTIVITY PROFILE

```
' PROGRAM:  HGHMCRV2
'
'   This program takes inputs of wind speed (kts), sea and air
'   temperature (deg C), and IR instrument height (m) and calculates the
'   M-profile for optical refractivity based on the formulation of
'   Businger, and estimates the depression angle for the horizon ray.
'
'this routine tests hardware to set either CGA, EGA4, or EGA16
'
ON ERROR GOTO CGA: SCREEN 9
ON ERROR GOTO EGA: COLOR 4
Mode$ = "EGA16": GOTO ENDSET
CGA:    Mode$ = "CGA": RESUME ENDSET
EGA:    Mode$ = "EGA4": RESUME ENDSET
ENDSET: ON ERROR GOTO 0
IF Mode$ = "CGA" THEN SCREEN 2 ELSE SCREEN 9
IF Mode$ <> "CGA" THEN PALETTE
IF Mode$ = "CGA" THEN PRINT "CGA MODE SELECTED"
IF Mode$ = "EGA4" THEN PRINT "4-COLOR EGA MODE SELECTED"
IF Mode$ = "EGA16" THEN PRINT "16-COLOR EGA MODE SELECTED"
Time0 = TIMER
Pause: IF TIMER < Time0 + 1 THEN GOTO Pause

DIM M(50), H(50)

Z0 = .00015       ' surface roughness parameter (m)
Z1 = 6            ' reference height (m)
k = .4            ' von Karmen's constant
PI = 3.14159


Top:

 CLS
 IF Mode$ <> "CGA" THEN COLOR 7
 LOCATE 1, 1
 INPUT "Enter wind speed (knots)"; Ws
 INPUT "Enter sea temperature (deg C)"; Ts
 INPUT "Enter air temperature (deg C)"; Ta
 INPUT "Enter IR receiver height (m)"; Hir
 CLS
'
 Tak = Ta + 273.2
 Tsk = Ts + 273.2
'
Rib = 369 * Z1 * (Tak - Tsk) / (Tak * Ws * Ws)
'
'     compute the Gamma function
```

```
'
 IF Rib <= -3.75 THEN
    Gamma = .05
 ELSEIF Rib <= -.12 THEN
    Gamma = .065 + Rib * .004
 ELSEIF Rib <= .14 THEN
    Gamma = .109 + Rib * .367
 ELSE
    Gamma = .155 + Rib * .021
 END IF

 Olp = Rib / (10 * Z1 * Gamma)
'
'      compute potential refractivity difference
'
 NA = 77.6 / Tak * (1000)
 N0 = 77.6 / Tsk * (1000)
 Deln = NA - N0
'
'      compute potential refractivity scaling parameter
'
 IF Ta < Ts THEN              ' unstable
'
    Psi = 2 * LOG(.5 * (1 + SQR(1 - 16 * Z1 * Olp)))
'
 ELSEIF Ta > Ts THEN          ' stable
'
    Psi = -5.2 * Z1 * Olp
'
 ELSE
'
    Psi = 0
'
 END IF
'
 Npstar = k * Deln / (LOG((Z1 + Z0) / Z0) - Psi)
'

 H(1) = 0
 M(1) = N0

 Lnminz = -2: Lnmaxz = 4: Inc = .5
 I = 1
 SELECT CASE Olp               ' 1/L'

   CASE IS >= 0                '  neutral and stable
'
'          calculate IR duct height
'
      Condition$ = "IR duct height ="
      DelIR = -Npstar / (.134 * k + 5 * Npstar * Olp)
'
'          calculate profile
'
```

```
      FOR Lnz = Lnminz TO Lnmaxz STEP Inc
         Z = EXP(Lnz)
         I = I + 1
         H(I) = Z
         M(I) = M(1) + .134 * Z
         M(I) = M(I) + Npstar / k * (LOG((Z + Z0) / Z0) + 5.2 * Z * Olp)
      NEXT Lnz
      Mhir = M(1) + .134 * Hir
      Mhir = Mhir + Npstar / k * (LOG((Hir + Z0) / Z0) + 5.2 * Hir * Olp)
      Imax = I
'
   CASE IS < 0                              ' unstable
'
'        calculate IR subrefractive layer height
'
      Condition$ = "IR subrefractive layer height ="
'              newton iteration for DelIR
      C = (Npstar / (.023 * .4)) ^ 2
      D1 = 0
      D2 = 10
      WHILE ABS(D2 - D1) > .001
         D1 = D2
         F = D1 ^ 2 - 16 * D1 ^ 3 * Olp - C
         Fp = 2 * D1 - 48 * D1 ^ 2 * Olp
         D2 = D1 - F / Fp
      WEND
      DelIR = D1
'
'        calculate profile
'
      FOR Lnz = Lnminz TO Lnmaxz STEP Inc
         Z = EXP(Lnz)
         I = I + 1
         H(I) = Z
         Psi = 2 * LOG(.5 * (1 + SQR(1 - 16 * Z * Olp)))
         M(I) = M(1) + .134 * Z + Npstar / k * (LOG((Z + Z0) / Z0) - Psi)
      NEXT Lnz
      Mhir = M(1) + .134 * Hir + Npstar / k * (LOG((Hir + Z0) / Z0) - Psi)
      Imax = I
'
 END SELECT

   PRINT "U="; Ws; "kts  Ts="; Ts; "C  Ta="; Ta; "C ";
   PRINT USING "  Rib = ###.####"; Rib;
   PRINT USING "  Z1/L = ###.####"; Z1 * Olp
'
LOCATE 3, 63: PRINT "  H(m)      M";
FOR I = 1 TO Imax
   LOCATE I + 4, 63
   PRINT USING "###.###  ####.##"; H(I); M(I)
NEXT I
'
'    find minimum on M-profile
'
```

```
Mmin = M(1)
FOR I = 2 TO Imax
   IF M(I) < Mmin THEN Mmin = M(I)
NEXT I
'
'     calculate approximate horizon ray depression angle
'
alpha = -SQR(.000002 * (Mhir - Mmin))
IF Mmin < M(1) THEN alpha = alpha - .000001
LOCATE 2, 15: PRINT USING "alpha = +##.###"; alpha * 1000;
PRINT " mrad";
'
'     scale and plot M
'
IF Mode$ = "CGA" THEN VIEW (32, 20)-(492, 180) ELSE VIEW (32, 32)-(492, 315)
IF Mode$ <> "CGA" THEN COLOR 7
Zs = 50
Min = INT(N0 - 5): Max = INT(M(Imax) + 1)
WINDOW (Min, 0)-(Max, Zs)
LINE (Min, Zs)-(Min, 0)
'  LINE (Min, 0)-(Max, 0)
FOR X = Min TO Max
   LINE (X, 0)-(X, .3 * Zs / 20)
   IF X MOD 5 = 0 THEN LINE -(X, .6 * Zs / 20)
NEXT X
LOCATE 24, 3: PRINT USING "###.#"; Min;
LOCATE 24, 34: PRINT "M";
LOCATE 24, 61: PRINT USING "###.#"; Max;
FOR Y = 0 TO Zs
   LINE (Min, Y)-(Min + (.25 * (Max - Min) / 25), Y)
   IF Y MOD 5 = 0 THEN LINE -(Min + (.5 * (Max - Min) / 25), Y)
NEXT Y
Row = -1
FOR I = 50 TO 0 STEP -10
   LOCATE Row + 4, 1: PRINT I;
   Row = Row + 4
NEXT I
IF Mode$ <> "CGA" THEN COLOR 14
PSET (M(1), H(1))
FOR I = 2 TO Imax
   LINE -(M(I), H(I))
NEXT I
'
LOCATE 25, 10: PRINT Condition$; : PRINT DelIR; : PRINT " m";
'
Spin: A$ = INKEY$: IF A$ = "" THEN GOTO Spin
'
IF Mode$ <> "CGA" THEN COLOR 7
VIEW
GOTO Top

END
```

REPORT DOCUMENTATION PAGE

Form Approved
OMB No. 0704-0188

1. AGENCY USE ONLY *(Leave blank)*	2. REPORT DATE	3. REPORT TYPE AND DATES COVERED
	October 1991	Final: Oct 1990—Sep 1991

4. TITLE AND SUBTITLE

VALIDATION OF THE BULK METHOD FOR OVERWATER OPTICAL REFRACTIVITY

5. FUNDING NUMBERS

PE: 0602435N
Proj: RU35G80
WU: 54 SXB3 01
Agency Accession No.: DN888715

6. AUTHOR(S)

R. A. Paulus

7. PERFORMING ORGANIZATION NAME(S) AND ADDRESS(ES)

Naval Ocean Systems Center
San Diego, CA 92152–5000

8. PERFORMING ORGANIZATION *REPORT NUMBER*

Technical Report 1462

9. SPONSORING/MONITORING AGENCY NAME(S) AND ADDRESS(ES)

Office of Naval Technology (ONT 21)
800 N. Quincy
Arlington, VA 22217

10. SPONSORING/MONITORING AGENCY REPORT NUMBER

11. SUPPLEMENTARY NOTES

12a. DISTRIBUTION/AVAILABILITY STATEMENT

Approved for public release; distribution is unlimited.

12b. DISTRIBUTION CODE

13. ABSTRACT *(Maximum 200 words)*

The effects of refraction on optical propagation at low altitudes over the ocean were investigated. A telescope was used to optically track ships to the range at which they disappeared over the horizon. Concurrent bulk meteorological measurements were used with surface-layer theory to model optical refractivity. A ray-trace program, with these profiles of refractivity, was used to calculate maximum intervision range (MIVR). Calculated MIVRs agree well with observations for subrefractive conditions (air cooler than water) typical of the open ocean. Agreement is not as good for super-refractive and ducting conditions (air warmer than water), which occurred with offshore flow and are therefore not typical of open ocean. Optical ducting conditions also appear to vary with range, such that point meteorological measurements and homogeneous ray tracing are not representative.

14. SUBJECT TERMS

overwater optical refractivity
bulk method
refraction
optical propagation
ship targets
surface-layer theory
ray-trace programs
maximum intervision range (MIVR)
optical ducting
meteorology

15. NUMBER OF PAGES

39

16. PRICE CODE

17. SECURITY CLASSIFICATION OF REPORT	18. SECURITY CLASSIFICATION OF THIS PAGE	19. SECURITY CLASSIFICATION OF ABSTRACT	20. LIMITATION OF ABSTRACT
UNCLASSIFIED	UNCLASSIFIED	UNCLASSIFIED	SAME AS REPORT

21a. NAME OF RESPONSIBLE INDIVIDUAL	21b. TELEPHONE *(include Area Code)*	21c. OFFICE SYMBOL
R. A. Paulus	(619) 553–1424	Code 543

INITIAL DISTRIBUTION

Code 0012	Patent Counsel	(1)
Code 0144	R. November	(1)
Code 54	J. H. Richter	(10)
Code 543	R. A. Paulus	(20)
Code 952B	J. Puleo	(1)
Code 961	Archive/Stock	(6)
Code 964B	Library	(3)

Defense Technical Information Center
Alexandria, VA 22304-6145 (4)

NOSC Liaison Office
Arlington, VA 22217

Center for Naval Analyses
Alexandria, VA 22302-0268

Navy Acquisition, Research & Development
Information Center (NARDIC)
Alexandria, VA 22333

Navy Acquisition, Research & Development
Information Center (NARDIC)
Pasadena, CA 91106-3955

Naval Research Laboratory
Washington, DC 20375-5000 (2)

Naval Surface Warfare Center
Silver Spring, MD 20910

Naval Postgraduate School
Monterey, CA 93940